

This is an Open Access document downloaded from ORCA, Cardiff University's institutional repository:<https://orca.cardiff.ac.uk/id/eprint/129414/>

This is the author's version of a work that was submitted to / accepted for publication.

Citation for final published version:

Li, Wei, Alves, Tiago M. , Rebesco, Michele, Sun, Jie, Li, Jian, Li, Shuang and Wu, Shiguo 2020. The Baiyun Slide Complex, South China Sea: a modern example of slope instability controlling submarine-channel incision on continental slopes. *Marine and Petroleum Geology* 114 , 104231. 10.1016/j.marpetgeo.2020.104231

Publishers page: <http://dx.doi.org/10.1016/j.marpetgeo.2020.104231>

Please note:

Changes made as a result of publishing processes such as copy-editing, formatting and page numbers may not be reflected in this version. For the definitive version of this publication, please refer to the published source. You are advised to consult the publisher's version if you wish to cite this paper.

This version is being made available in accordance with publisher policies. See <http://orca.cf.ac.uk/policies.html> for usage policies. Copyright and moral rights for publications made available in ORCA are retained by the copyright holders.



1 **The Baiyun Slide Complex, South China Sea: A modern example of slope**
2 **instability controlling submarine-channel incision on continental slopes**

3
4 Wei Li^{a, b, c*}, Tiago M. Alves^d, Michele Rebesco^e, Jie Sun^{a, b*}, Jian Li^{a, c}, Shuang Li^{a, c}, Shiguo Wu^f

5
6 ^a CAS Key Laboratory of Ocean and Marginal Sea Geology, South China Sea Institute of
7 Oceanology, Chinese Academy of Sciences, Guangzhou 510301, P. R. China

8 ^b Innovation Academy of South China Sea Ecology and Environmental Engineering, Chinese
9 Academy of Sciences, Guangzhou 510301, P. R. China

10 ^c University of Chinese Academy of Sciences, Beijing 100049, P.R. China

11 ^d 3D Seismic Lab. School of Earth and Ocean Sciences, Cardiff University, Main Building, Park
12 Place, Cardiff, CF10 3AT, United Kingdom

13 ^e Istituto Nazionale di Oceanografia e di Geofisica Sperimentale (OGS), Borgo Grotta Gigante 42/C,
14 Sgonico, 34010 Trieste, Italy

15 ^f Institute of Deep-sea Science and Engineering, Chinese Academy of Sciences, Sanya 572000, P. R.
16 China

17 *Corresponding author: Dr. Wei Li (wli@scsio.ac.cn) and Dr. Jie Sun (sunjie@scsio.ac.cn)

18
19 **Abstract**

20 The Baiyun Slide Complex is one of the largest known submarine landslides on the northern margin
21 of the South China Sea. Newly acquired high-resolution bathymetric data, 2D and 3D seismic data
22 permitted the systematic investigation of the Baiyun Slide Complex in terms of its seafloor
23 morphology and associated sedimentary processes. The headwall region of the Baiyun Slide
24 Complex, located at a water depth between 1000 m and 1700 m, is U-shaped and opens towards the

25 east. It was efficiently and almost completely evacuated, generating pronounced headwall and
26 sidewall scarps. Submarine channels, sediment waves, migrating channels, sediment drifts and
27 moats can be observed within and around the headwall region, illustrating the effects of both
28 downslope and along-slope sedimentary processes. Submarine channels are 16-37 km-long
29 800-1500 m-wide, and 20 to 50 m-deep. As a modern example of the interplay between slope
30 instability and subsequent incision, submarine channels were generated after the formation of the
31 Baiyun Slide scar to suggest intensified downslope sedimentary processes after the slope collapsed.
32 The initiation and formation of these submarine channels are suggested to result from the
33 evacuation of the Baiyun Slide scar, which provided accommodation space for subsequent turbidity
34 currents and mass wasting. Our results are an important example of how submarine landslides can
35 influence erosional and depositional processes on continental margins.

36

37 **Keywords:** South China Sea; Submarine landslide; submarine channels; bottom currents; turbidity
38 currents.

39

40 **1. Introduction**

41 Submarine landslides, turbidity currents and bottom currents are dominant sedimentary
42 processes occurring along both passive and active continental margins (Vorren et al., 1998; Rebesco
43 et al., 2014; Mosher et al., 2017). Downslope processes such as landslides and turbidity currents are
44 driven by gravity and lead to the deposition of broad mass-transport deposits or turbidite systems
45 within erosive channels (Moscardelli et al., 2006; Casalbore et al 2010; Bourget et al., 2011; Li et
46 al., 2015b). They can transport large volumes ($>100 \text{ km}^3$) of sediment sourced from the continental
47 shelf and upper slope areas into the deep ocean (Georgiopoulou et al., 2010; Li et al., 2018),

48 re-shaping the sea floor to influence subsequent sedimentary processes (Casalbore et al 2018). They
49 can also control the distribution of sand in deep-water environments (Haflidason et al., 2004;
50 Mosher et al., 2017). Along-slope bottom currents result in extensive depositional (e.g. sediment
51 drifts) and erosional (e.g. contourite channels) features on outer continental shelves and upper
52 continental slopes (Hernández-Molina et al., 2006; García et al., 2009; Rebesco et al., 2013). A
53 close interplay between downslope turbidity currents and alongslope contour currents is therefore
54 expected when both processes occur on continental margins (Rebesco et al., 2002; Caburlotto et al.,
55 2006; Brackenridge et al., 2013; Martorelli et al 2016).

56 The continental margin offshore the Pearl River Mouth Basin (PRMB) is incised by deep-water
57 submarine canyons and channels (Zhu et al., 2010). The most striking feature in the PRMB is the
58 Baiyun Slide Complex, which has a large spatial coverage (~10,000 km²) and is composed of
59 several intersecting slide scars and overlapping deposits (Li et al., 2014; Sun et al., 2018b) (Fig. 1).
60 The total volume of sediment removed by the Baiyun Slide Complex is ~1035 km³ and comprises
61 four major mass-transport deposits (MTDs) separated by basal erosional surfaces (Sun et al., 2018b).
62 These MTDs retrograded upslope to reveal a decreasing time interval between events (Wang et al.,
63 2017; Sun et al., 2018b). Two main instability events occurred in the headwall region of the Baiyun
64 Slide Complex during the Quaternary (Li et al., 2014; Wang et al., 2017; Sun et al., 2018b), at
65 ~0.79 Ma and ~0.54 Ma (Sun et al., 2018b). The older MTD (1570 km²) covers most of the
66 headwall region, while the younger MTD is mainly limited to the northern area of the headwall
67 region to reveal a relatively smaller area of ~ 840 km² (Wang et al., 2017).

68 The study area is chiefly located in the headwall region of the Baiyun Slide Complex, at a
69 water depth of 900 m to 1800 m (Figs. 2a and b). This region is affected by alongslope bottom
70 currents associated with a clockwise flow of intermediate water at a depth of 350 m to 1350 m, and

71 an anticlockwise flow of deep water at depths beyond 1350 m (Gong et al., 2013; Chen et al., 2014)
72 (Fig. 1). Thus, it provides a key opportunity to characterise how bottom currents, turbidity currents
73 and submarine landslides influence the morphological and sedimentary evolution of the northern
74 South China Sea margin.

75 High-resolution bathymetric, 2D/3D seismic and borehole data are used to provide a detailed
76 analysis of erosional and depositional features in and around the headwall region of Baiyun Slide
77 Complex. The specific aims of this research are to:

78

- 79 a) investigate the seafloor morphology in and around the headwall region of the Baiyun Slide;
- 80 b) describe the internal seismic characters of the Baiyun Slide, and determine what are the main
81 sedimentary processes in this area;
- 82 c) discuss the role of the Baiyun Slide Complex on the incision and development of submarine
83 channels.

84

85 **2. Geological and oceanographic background**

86

87 *2.1 Geological setting*

88 The South China Sea is one of the largest (and deepest) marginal seas in the western Pacific
89 Ocean (Fig. 1). The formation of the South China Sea as observed at present involved the formation
90 of a proto-South China Sea, likely floored by oceanic crust, that was subducted during the Mesozoic
91 (Pubellier et al., 2003). The earliest phase of rifting in South China Sea started in the latest
92 Cretaceous to Early Paleocene and, after ~30 Ma of rifting, continental breakup occurred first in its
93 Eastern Sub-basin in the Early Oligocene before ~32 Ma (Barckhausen et al., 2013; Briais et al.,

94 1993). Continued continental rifting led to breakup of the Southwest Sub-basin in the Late
95 Oligocene at ~25 Ma. In parallel to continental breakup, seafloor spreading in the South China Sea
96 started during the Early Oligocene before terminating in the Late Oligocene (Li et al., 2015a).
97 Seafloor spreading in the South China Sea thus spans from 33 Ma to 15 Ma in the Northeast
98 Sub-basin, and from 23.6 Ma to 16 Ma in the Southwest Sub-basin, respectively, based on the new
99 results at IODP Site U1435 (Li et al., 2015a).

100 The northern South China Sea margin has been influenced by seasonal alternations of the East
101 Asian summer monsoon and the East Asian winter monsoon sub-regimes since, at least, the Late
102 Miocene (Steinke et al., 2010). The rate and composition of terrigenous sediment supplied to
103 continental shelves, continental slopes and deep-sea basins has been largely influenced by changing
104 monsoon conditions (Steinke et al., 2003; Steinke et al., 2006). Intensified winter monsoon winds
105 can increase wave heights in coastal zones, further amplifying sediment reworking processes. In
106 such a setting, fine-grained fluvial sediment can be suspended in the water column to bypass the
107 outer shelf and settle on the continental slope (Steinke et al., 2003; Steinke et al., 2010).

108 The PRMB lies in the central part of the northern South China Sea and it is one of the most
109 important hydrocarbon-rich basins in the region (Fig. 1). The geological evolution of the PRMB
110 comprised three main stages: (1) a first rifting stage in the Late Cretaceous-Early Oligocene,
111 essentially marked by continental rifting; (2) a transitional stage (Late Oligocene-Early Miocene)
112 recording syn-rift faulting, subsidence and deposition within distinct sub-basins; (3) a post-rift stage
113 from the Middle Miocene to Holocene dominated by post-rift subsidence and filling of syn-rift
114 basins (Gong et al., 1989). In the PRMB, regional tectonic uplift, faulting, erosion and magmatism
115 are recorded in association with major tectonic events (Wu et al., 2014; Zhao et al., 2016). The most
116 prominent tectonic event in the study area, the Dongsha Event, started in the Late Miocene (T2:

117 10.5 Ma; Fig. 3) and ceased around the Miocene/Pliocene boundary, at around 5.5 Ma (T1; Fig. 3;
118 Wu et al., 2014). As a result, a deep-water depositional setting was gradually developed after the
119 Early Miocene, originating multiple submarine canyons, submarine channels on the continental
120 slope and associated deep-water sediment fans (Fig. 3; Xie et al., 2006).

121

122 *2.2 Oceanographic setting*

123 Water masses in the South China Sea include a seasonally-influenced surface water and
124 permanent intermediate- and deep-water masses (Tian et al., 2006; Chen et al., 2014) (Fig. 1).
125 Surface water is controlled by the East Asia monsoon system and occurs at a water depth less than
126 350 m (Lüdmann et al., 2005; Contreras-Rosales et al., 2019). Surface water is clockwise during the
127 summer and counterclockwise during the winter (Zhu et al., 2010). Intermediate water
128 (350 m-1350 m) follows a permanent clockwise movement and corresponds to the western
129 boundary current in the South China Sea (Tian et al., 2006). It was established in the Late Miocene,
130 resulting in: 1) the development of unidirectionally migrating deep-water channels in the Pearl
131 River Mouth Basin (Zhu et al., 2010; Gong et al., 2013), 2) the subsequent formation of
132 depositional and erosional patterns around the South Shenhu Seamount (Chen et al., 2014) (Fig. 1).
133 Deep water originates from the incursion of the southward flowing North Pacific Deep Water into
134 the South China Sea via the Luzon Strait (Lüdmann et al., 2005). Widespread and thick sediment
135 drifts occur to the southeast of the Dongsha Islands in association with deep-water currents, in
136 places recording a maximum velocity of ~30 cm/s (Zhao et al., 2014).

137

138 **3. Data and methods**

139 High-resolution multibeam bathymetric data, 2D seismic profiles and 3D seismic volumes are

140 used in this work. The bathymetric data was acquired at water depths ranging from 230 m to 2600
141 m using differential GPS positioning. It was processed using the software CARIS HIPS[®]. Its
142 horizontal and vertical resolutions are ~100 m and ~1-3.3 m, respectively, enabling the
143 identification and analysis of seafloor features generated by downslope and alongslope currents.

144 The interpreted seismic dataset was acquired and processed by China National Offshore Oil
145 Corporation (CNOOC) and covers the headwall region of the Baiyun Slide Complex. It consists of
146 one long (~100 km) 2D seismic profile crossing submarine canyons and channels on the continental
147 slope, and ~4000 km² of 3D seismic data. The dominant frequency of the 2D seismic data is ~30 Hz,
148 and its vertical resolution ranges from 15 to 20 m. The 3D seismic data has a dominant frequency of
149 40-60 Hz in the interval of interest, providing a vertical resolution of about 10-15 m. This relatively
150 high resolution of the seismic data enabled the detailed investigation of sedimentary features in the
151 headwall region of Baiyun Slide Complex (Fig. 4a).

152 Exploration Well L-13 was drilled in the central part of the study area and provided age
153 constrains for the interpreted seismic horizons (Fig. 2a). Main seismic reflections were identified
154 and traced using Schlumberger's Geoframe[®] 4.5 so that a regional seismic-stratigraphic framework
155 could be built for the study area. Three important seismic horizons (T0, T1 and T2) were recognised
156 and dated as 1.9 Ma, 5.5 Ma and 10.5 Ma in age (Fig. 4a).

157

158 **4. Seismic stratigraphy**

159 The seismic stratigraphy of the study area was interpreted and tied to borehole data from
160 Exploration Well L-13. Three main seismic units, named as Units A, B and C from top to bottom,
161 were identified based on the differences in their internal reflection configurations (Figs. 4a and b).

162 Unit A is bounded by T0 at its base and its top coincides with the sea floor (Fig. 4a). Unit A is

163 suggested to be Quaternary in age. On the upper continental slope, moderate- to high-amplitude
164 reflections predominate (Fig. 4a). Downslope, widespread chaotic seismic reflections suggest the
165 presence of MTDs (Fig. 4d). The most prominent feature in Unit A is the slide scar from the Baiyun
166 Slide Complex, herein named Baiyun Slide scar, and MTDs resulting this latter instability feature
167 (Fig. 4b).

168 Unit B is Pliocene in age and bounded by seismic horizons T1 and T0 (Figs. 4a and b). Seismic
169 facies in Unit B change in different parts of the study area (Fig. 4a). In the upper slope region,
170 several submarine canyons can be identified (Figs. 4a and c). In the middle sector of the slope, Unit
171 B shows continuous and moderate-amplitude reflections (Fig. 4a). Strata downslope from this latter
172 region shows chaotic seismic reflections bounded by irregular top and bottom surfaces (Figs. 4a and
173 d), likely comprising MTDs. Unit B shows variable thickness in the E-W seismic profile in Fig. 4a.

174 Unit C is bounded by seismic horizon T2 at its bottom and T1 at its top. Unit C is Late Miocene
175 in age and shows low- to moderate-amplitude reflections (Figs. 4a and b). A main valley and several
176 buried submarine canyons are observed in the middle part of Unit C (Fig. 4a). The thickness of Unit
177 C is variable on the E-W seismic profile in Fig. 4a, but shows a constant thickness on the SW-NE
178 oriented seismic profile in Fig. 4b. Several large-scale faults can be observed cutting through Unit
179 C.

180 **5. Seafloor morphology**

181 Seafloor morphology is uneven in the study area (Figs. 2a and 5a). Different kinds of
182 morphological features can be identified, with the most prominent feature being the Baiyun Slide
183 scar (Fig. 2a).

184

185 *5.1 Baiyun Slide scar*

186 The headwall region of the Baiyun Slide Complex displays a U-shaped slide scar that opens
187 towards the east with a length of ~50 km and an average width of 14 km (Figs. 2a and 5a). This scar
188 is located at a water depth between 1100 m and 1600 m, and covers ~700 km² in area (Figs. 2a and
189 b). The northern escarpment of the scar is ~45 km in length and consists of several smaller-scale
190 scars (Fig. 5a). In the south, the escarpment shows a length of ~50 km and appears to be disrupted
191 by several ridges. The headwall scarp has an average height of ~90 m and a slope gradient of up to
192 19° (Figs. 2a and 4a). The escarpment of the slide scar is much steeper in the north (up to 22°) than
193 in the south (~5°), as shown on the bathymetric profiles crossing the slide scar (Figs. 5b and c). The
194 undeformed seafloor has a gradient of ~1° (Fig. 5a).

195

196 *5.2 Submarine canyons and channels*

197 Submarine canyons are usually not connected to a modern river, and have nearly vertical and
198 steep walls that extend well onto the continental shelf. Submarine channels are smaller, usually
199 meandering, and comprise a thalweg and confining levees (Shepard, 1936; Shepard, 1981; Amblas
200 et al., 2018). They are much less steep than canyons and are commonly within canyons themselves -
201 it is not uncommon to record channel systems at the bottom of canyons. To the north of the
202 headwall area of the Baiyun Slide Complex occur seventeen (17) submarine canyons, as already
203 documented by Zhu et al. (2010), Gong et al. (2013) and Ma et al. (2015). In this study, only seven
204 of these canyons are fully imaged on the newly-acquired bathymetric data, towards the western part
205 of the complex (Fig. 2a). The orientation of these submarine canyons is NNW-SSE, and is
206 perpendicular to the continental slope. These submarine canyons are sub-linear and sub-parallel in
207 plan view, displaying a regular spacing of 8 to 10 km. They are located at water depths ranging

208 from 500 m to 1500 m (Fig. 2b). As observed on the contour map in Fig. 2b, these submarine
209 canyons are confined on the continental slope and do not erode the shelf edge, which occurs at a
210 water depth of ~200 m. These submarine canyons are about 20-40 km-long, 3-5 km-wide and incise
211 the slope to a depth of 100-300 m. The bathymetric profile crossing the submarine canyons shows
212 that canyon flanks are steep and display V-shaped geometries (Fig. 6a). Compared to the large-scale
213 submarine canyons, several small-scale submarine channels (A1 to A6) can be clearly distinguished
214 on the upper continental slope above the headwall region (Figs. 2a, 6b and 6c; Table 1). These
215 submarine channels are 16-37 km-long, 800-1500 m-wide and 20 to 50 m-deep (. 6b). Some of
216 these channels (A2-A3 and A4-A5) incise the headwall scarp to extend into the upper part of the
217 Baiyun Slide Complex (Figs. 2a and 5a).

218

219 **6. Morphology and internal character of the Baiyun Slide scar**

220

221 *6.1 Slide scarps and mass-transport deposits (MTDs)*

222 The headwall and sidewall scarps of the Baiyun Slide Complex can be readily identified on the
223 bathymetric map and seismic profiles (Figs. 2a, 4a and 7a). The slide scarps are steep and adjacent
224 intact strata show obvious erosional truncations (Figs. 4b and 7b). Most MTDs are located in Units
225 A and B, especially downslope from the slide headwall where recurrent MTDs are observed (Figs.
226 4a and c). The uppermost MTD shows a thickness of ~75 m (Figs. 4c and d). Beneath this MTD,
227 several smaller-scale MTDs are vertically stacked and naturally increase the total thickness of
228 mass-wasting deposits on the continental slope (Fig. 4c). Compared to the seismic profiles imaging
229 the lower continental slope, relatively thin MTDs can be identified within the headwall area of the
230 Baiyun Slide Complex (Figs. 7a and c).

231

232 *6.2 Erosive channels and moats*

233 Six submarine channels are observed on the bathymetric map and on seismic data (Figs. 4b, 6b,
234 7 and 8). A submarine channel (A2-3 generated by the confluence of channels A2 and A3) is
235 incising the seafloor of the uppermost (westward) part of the Baiyun Slide Complex (Figs. 5a and b).
236 This channel has a width of approximately 2 km and a depth of about 50 m (Figs. 5b and 8a). It cuts
237 the headwall scarp of the Baiyun Slide Complex and extends farther towards the east. Seismic
238 reflections crossing the submarine channel are not continuous, and erosional truncations can be
239 observed on both flanks of the channel (Figs. 8c and d). Another two erosive channels are located in
240 the southern part of its headwall region (Fig. 5a). They both have an E-W orientation, parallel to the
241 southern escarpment of the slide scar.

242 Elongated depressions can be observed on the bathymetric map and seismic profiles located in
243 the vicinity of the slide scarps (Figs. 8a, b and c). Strata close to these depressions typically exhibit
244 a mounded shape (Fig. 8c). Such features can be interpreted as moats, i.e. localised erosional
245 features with little effect other than forming channeled paths for sediment that is redistributed along
246 the slope (Rebesco et al., 2007; García et al., 2009). Mounded strata comprise sediment drifts (Figs.
247 7b and 8c), as their most distinctive feature is the termination of internal reflections towards the
248 moat (Rebesco et al., 2016).

249

250 *6.3 Sediment waves*

251 Sediment waves are observed at different locations within and around the Baiyun Slide
252 Complex, such as those within the slide scar (Fig. 7c) and south of the slide scar (Figs. 9a, b and
253 10b). Internal seismic reflections within the sediment waves are continuous, showing moderate to

254 low amplitude (Figs. 10a and b). Continuous internal reflections can be traced across adjacent
255 waves. Sediment waves show a variety of dimensions, wavelengths ranging from 2 km to 4 km, and
256 wave heights between 30 m and 70 m. The crests of sediment waves within the slide scar typically
257 show upslope migration trends (Fig. 10a). Also, these sediment waves have asymmetric geometries.
258 The sediment waves in the south of the slide scar are dominated by vertical aggradation, rather than
259 upslope migration (Fig. 10b). Deposition occurs both on their upslope and the downslope flanks.
260 Individual sediment waves are usually symmetric.

261

262 *6.4 Migrating channels*

263 Buried channels are widely observed and some show typical unidirectional migration (Figs. 7b
264 and 11). Buried migrating channels are located in the southern part of the headwall region. The
265 channels are marked at their base by a basal erosional unconformity, which is marked by a
266 continuous and high-amplitude concave upwards reflection (Fig. 11). The thalweg of a buried
267 channel in the shallower area (water depth <1500 m) is progressively offset towards the north and
268 the unidirectional migration distance of its thalweg reaches 3 km (Fig. 11). In parallel, MTDs are
269 observed within the channel and are likely the main depositional elements of the channel fills (Fig.
270 11).

271

272 **7. Discussion**

273 *7.1 Importance of combined downslope and alongslope processes on a sediment-fed continental* 274 *slope*

275 We propose that the headwall region of the Baiyun Slide Complex was affected by both

276 downslope and alongslope sedimentary processes since its inception as: (a) it is located at a water
277 depth influenced by bottom currents associated with intermediate (350 m-1350 m) and deep-water
278 circulation (>1350 m); and (b) it is close to submarine canyons incising the continental slope at the
279 same place where submarine slides and turbidity currents occurred frequently in the past. In this
280 work, several types of depositional and erosional features are identified, demonstrating the
281 influence of turbidity currents, contour currents and sediment mass-wasting on the geomorphology
282 of the headwall of the Baiyun Slide Complex, and around it.

283 MTDs are mainly identified in Unit A and B, indicating that downslope sedimentary processes
284 have been active since the end of the Late Miocene. The uppermost two MTDs have been
285 interpreted as the slide deposits of the last stages of instability in the Baiyun Slide Complex (Li et
286 al., 2014; Wang et al., 2017; Sun et al., 2018b), and were respectively dated as 0.54 Ma and 0.79
287 Ma based on seismic-stratigraphy correlations with ODP Site 1146 (Sun et al., 2017). The other
288 MTDs are noticeably smaller and might have been sourced from adjacent submarine canyons.
289 Multiple scars of submarine landslides associated with submarine canyons have been mapped in
290 this region, being bounded by headscarps and basal shear surfaces (He et al., 2014; Chen et al.,
291 2016). These submarine landslides are mostly distributed around the canyon heads and flanks, with
292 some having been able to further disintegrate and evolve into turbidity currents flowing along the
293 submarine canyons (Chen et al., 2016).

294 Buried sediment waves observed within the slide scar display asymmetric morphologies with
295 gentle upslope flanks and steep downslope flanks (Figs. 6c and 9a). These sediment waves have
296 thicker beds on their upcurrent face and their crests exhibit an upslope migration trend (Fig. 10a).
297 The internal seismic reflections within these sediment waves are continuous and can be traced from
298 one wave to the next. In addition, they are very close to the submarine canyons in the upper

299 continental slope where turbidity currents occur more frequently. Therefore, based on the criteria
300 of Wynn and Stow (2002), these sediment waves can be interpreted to have been formed by
301 turbidity currents flowing through submarine canyons on the upper continental slope. Once the
302 initial sediment wave topography is established, the process leading to wave migration and growth
303 is self-perpetuating (Normark et al., 2002). Sediment waves with similar internal seismic characters
304 have also been documented in the Magdalena turbidite system (Ercilla et al., 2002), on the South
305 Iberian Margin (Perez-Hernandez et al., 2014) and on the South China Sea slope offshore SW
306 Taiwan (Gong et al., 2012; Gong et al., 2015), where the genesis of sediment waves is considered to
307 result from turbidity currents. Additionally, erosive channels on the upper continental slope may
308 also be formed by the erosion of turbidity currents, which were probably initiated by the
309 transformation of slumps or storm-generated flows near the shelf edge (Figs. 2a and 7d).

310 Two moats and associated sediment drifts have been identified close to the slide scarps in the
311 headwall region of the Baiyun Slide (Figs. 4a and 7c), indicating enhanced activity of bottom
312 currents after the formation of the observed slide scar, as uneven seafloor bathymetry may locally
313 intensify and focus bottom-current activity (García et al., 2009; Vandorpe et al., 2016; Martorelli et
314 al 2016). The moats can also be used to reconstruct the path of the inferred bottom current flow that
315 controlled the development of sediment drifts (Surlyk and Lykke-Andersen, 2007; Rebesco et al.,
316 2016). The two erosive channels in the south of the slide scar are interpreted as contourite channels
317 as they are far away from the influence of turbidity currents (Figs. 2a, 6b, 8a and b). In comparison,
318 the sediment waves observed in the southern part of the slide scar are relatively more symmetric
319 with continuous, parallel to sub-parallel internal reflections, indicative of active vertical aggradation
320 rather than upslope migration (Figs. 8a and b). This internal character is consistent with that
321 observed from bottom-current sediment waves (Gong et al., 2015; Baldwin et al., 2017).

322 Of particularly interest is the identification on bathymetric data of an erosive channel to the
323 south of the Baiyun Slide scar (Fig. 5a). This channel has no obvious levee and its base migrates
324 progressively northwards (Figs. 7b and 11). It can be interpreted as an unidirectionally migrating
325 channel similar to those documented on the northern South China Sea margin (He et al., 2013;
326 Gong et al., 2013; Gong et al., 2018), on the continental rise of southeast Greenland (Rasmussen et
327 al., 2003) and along the continental margin of Equatorial Guinea (Jobe et al., 2011). The presence
328 of this unidirectionally migrating channel suggests a close interaction between episodic downslope
329 gravity or turbidity flows and persistent alongslope bottom (contour) currents.

330

331 *7.2 The role of slide scars on the initiation and formation of submarine channels*

332 The bathymetric map covering the headwall of the Baiyun Slide Complex reveals the presence
333 of several submarine channels (Figs. 4a and 5b). These submarine channels with a general NW-SE
334 orientation incise the headwall scarp of the Baiyun Slide Complex and erode the Baiyun Slide scar
335 farther – up to a maximum distance of 10 km from this latter (Figs. 2a, 5a and 6b). The submarine
336 channels are close to submarine canyons and have similar orientations (Fig. 2a).

337 The bathymetric profile crossing the submarine canyons and channels reveals conspicuous
338 differences in their scales and incision depths (Fig. 6a). Submarine canyons have developed, at least,
339 since the Middle Miocene (Gong et al., 2013; Ma et al., 2015), but the timing of formation of
340 channels has not been constrained in the literature. Truncations can be clearly observed on the
341 seismic profiles crossing the observed submarine channels (Figs. 4b, 7a and 8c), which eroded the
342 draped strata above the MTDs up to a depth of ~60 m (Fig. 5b). These data provide a robust proof
343 that these submarine channels were formed after the Baiyun Slide Complex was initiated (Fig. 4b).
344 Therefore, we propose that submarine channels identified around the Baiyun Slide scar are

345 relatively newly-formed erosional features compared to the longer-lived submarine canyons.

346 Based on the detailed interpretation of bathymetry and seismic data, we propose a conceptual
347 model to explain the morphological evolution of the study area (Fig. 12). The Baiyun Slide
348 Complex evacuated large volumes of sediment ($\sim 1035 \text{ km}^3$) and greatly changed the slope
349 morphology (Figs. 12a and b; Li et al., 2014; Sun et al., 2018a). In addition, the formation of the
350 Baiyun Slide scar was able to enhance local accommodation space for subsequent turbidity currents
351 and mass-wasting deposits (Figs. 12b and c). We therefore suggest that the formation of the Baiyun
352 Slide scar has played a vital role on the initiation and formation of the submarine channels
353 identified on the upper part of the slide scar. Qin et al. (2017) also found that slide scars can capture
354 turbidity flows and facilitate flow channelisation, both key processes for the initiation of submarine
355 channels in the Espírito Santo Basin, SE Brazil. In addition, Abdurrokhim and Ito (2013) have
356 investigated the role of slump scars as initial seabed features responsible for the formation of slope
357 channels in the Bogor Trough, West Java. Initial depressions or seafloor roughness induced by
358 slump scars and by mass-transport deposits may develop an area of sediment-gravity flow
359 convergence able to locally incise the slope to form submarine channels (Alves and Cartwright,
360 2010; Qin et al., 2017).

361 The submarine channels in the upslope region of Baiyun Slide scar are V-shaped in
362 cross-section (Figs. 4b, 5a and 6b) and their upper reaches are close to the shelf edge (Figs. 2a and
363 6a). Several other small-scale slide scarps close to the shelf edge are imaged on high-resolution
364 bathymetric data (Figs. 2a and 6b). They may result either from large, unconfined and erosive
365 turbidity currents or from mass wasting. In such a setting, channels are suggested to be the first
366 features to form on steeply dipping slopes sculpted by mass wasting (e.g. Lonergan et al., 2013;
367 Laberg et al., 2007). Micallef and Mountjoy (2011) have also proposed gravity flows to be

368 responsible for initiating V-shaped channels in the Cook Strait, New Zealand. The importance of
369 interaction between turbidity current processes and seafloor roughness on channel initiation has also
370 been stressed by Gee et al. (2007) and Covault et al. (2014). Hence, the incision of submarine
371 channels in the study area can be considered as an indicator of intensified downslope sedimentary
372 processes (e.g. turbidity currents and mass wasting) after the Baiyun Slide scar was formed. As for
373 the triggering factors increasing downslope sedimentary gravity flows, Wang et al. (2018) proposed
374 that the long-term erosion by contour currents associated with the South China Sea Branch of the
375 Kuroshio Current caused the slope to become unstable and prone to collapse.

376

377 **8. Conclusions**

378 High-resolution bathymetry and 2D/3D seismic data enabled us to investigate the headwall
379 region of Baiyun Slide Complex on the northern South China Sea in terms of its geomorphology,
380 associated sedimentary processes and its role on the initiation of submarine channels. The main
381 conclusions of this study are as follows:

382 (1) The headwall region of Baiyun Slide Complex has a U-shaped morphology in plan view at
383 a water depth between 1000 m and 1700 m. Sediment was almost completely evacuated from the
384 complex, leaving pronounced headwall and sidewall scarps.

385 (2) Sediment waves, moats, erosional channels and migrating channels were identified inside
386 and around the headwall of the Baiyun Slide Complex. Downslope and alongslope sedimentary
387 processes have controlled and affected the overall geomorphology inside and around the latter
388 headwall region.

389 (3) Sediment waves identified in the downslope from submarine canyons were generated by
390 turbidity currents, while those distinguished in the southern part of the Baiyun Slide scar were

391 generated by bottom currents interacting with the sea floor. The presence of migrating channels
392 reveals a close interaction between downslope and alongslope sedimentary processes.

393 (4) The submarine channels on the upper part of the Baiyun Slide scar were formed in the
394 Quaternary, after the formation of this latter bathymetric feature. The submarine channels are
395 proposed as indicating the intensification of downslope sedimentary processes (e.g. turbidity
396 currents and mass wasting) over alongslope processes after the Baiyun Slide scar was formed.

397 This research is an important case study of the role of submarine landslides on regional
398 sedimentary processes. Our results are also of importance to characterise the sedimentary processes
399 operating on continental margins where a close interplay between downslope and alongslope
400 currents occurred in the past.

401

402 **Acknowledgments**

403 We acknowledge China National Offshore Oil Corporation for their permission to release the seismic data.
404 Dr. Neil C. Mitchell is thanked for his invaluable assistance and fruitful discussion, which improved this paper.
405 This work was financially supported by the Innovation Development Fund of South China Sea
406 Eco-Environmental Engineering Innovation Institute of the Chinese Academy of Sciences (ISEE2018PY02),
407 National Scientific Foundation of China (41876054), National Key Research and Development Program of
408 China (2017YFC1500401) and Key Laboratory of Ocean and Marginal Sea Geology, Chinese Academy of
409 Sciences (OMG18-09). The bathymetric maps in this study were produced through Global Mapper 11 and Surfer
410 10. Dr. Wei Li is funded by CAS Pioneer Hundred Talents Program (Y8SL011001). The paper benefited from the
411 constructive comments of the editor, Dr. Daniele Casalbore and one anonymous reviewer.

412

413

414 **References**

- 415 Abdurrokhim, Ito, M., 2013. The role of slump scars in slope channel initiation: A case study from the Miocene
416 Jatiluhur Formation in the Bogor Trough, West Java. *Journal of Asian Earth Sciences* 73, 68-86.
- 417 Alves, T.M., Cartwright, J.A., 2010. The effect of mass-transport deposits on the younger slope morphology,
418 offshore Brazil. *Marine and Petroleum Geology* 27, 2027-2036.
- 419 Amblas, D., Ceramicola, S., Gerber, T.P., Canals, M., Chiocci, F.L., Dowdeswell, J.A., Harris, P.T., Huvenne,
420 V.A.I., Lai, S.Y.J., Lastras, G., Iacono, C.L., Micallef, A., Mountjoy, J.J., Paull, C.K., Puig, P., Sanchez-Vidal,
421 A., 2018. Submarine Canyons and Gullies, in: Micallef, A., Krastel, S., Savini, A. (Eds.), *Submarine*
422 *Geomorphology*. Springer International Publishing, Cham, pp. 251-272.
- 423 Baldwin, K.E., Mountain, G.S., Rosenthal, Y., 2017. Sediment waves in the Caroline Basin suggest evidence for
424 Miocene shifts in bottom water flow in the western equatorial Pacific. *Marine Geology* 393, 194-202.
- 425 Barckhausen, U., Engels, M., Franke, D., Ladage, S., Pubellier, M., 2014. Evolution of the South China Sea:
426 Revised ages for breakup and seafloor spreading. *Marine and Petroleum Geology* 58, 599-611.
- 427 Bourget, J., Zaragosi, S., Ellouz-Zimmermann, N., Mouchot, N., Garlan, T., Schneider, J.-L., Lanfumey, V.,
428 Lallemand, S., 2011. Turbidite system architecture and sedimentary processes along topographically complex
429 slopes: the Makran convergent margin. *Sedimentology* 58, 376-406.
- 430 Brackenkridge, R.E., Hernández-Molina, F.J., Stow, D.A.V., Llave, E., 2013. A Pliocene mixed contourite–turbidite
431 system offshore the Algarve Margin, Gulf of Cadiz: Seismic response, margin evolution and reservoir
432 implications. *Marine and Petroleum Geology* 46, 36-50.
- 433 Briais, A., Patriat, P., Tapponnier, P., 1993. Updated interpretation of magnetic anomalies and seafloor spreading
434 stages in the South China Sea: implications for the Tertiary tectonics of Southeast Asia. *J. Geophys. Res.* 98,
435 6299–6328.
- 436 Caburlotto, A., De Santis, L., Zanolli, C., Camerlenghi, A., Dix, J.K., 2006. New insights into Quaternary glacial

437 dynamic changes on the George V Land continental margin (East Antarctica). *Quaternary Science Reviews*
438 25, 3029-3049.

439 Casalbore, D., Martorelli, E., Bosman, A., Morelli, E., Latino Chiocci, F., 2018. Failure dynamics of landslide
440 scars on the lower continental slope of the Tyrrhenian Calabrian margin: insights from an integrated
441 morpho-bathymetric and seismic analysis. *Geological Society, London, Special Publications 477, SP477.416.*

442 Casalbore, D., Romagnoli, C., Chiocci, F., Frezza, V., 2010. Morpho-sedimentary characteristics of the
443 volcanoclastic apron around Stromboli volcano (Italy). *Marine Geology 269, 132-148.*

444 Chen, D., Wang, X., Völker, D., Wu, S., Wang, L., Li, W., Li, Q., Zhu, Z., Li, C., Qin, Z., Sun, Q., 2016. Three
445 dimensional seismic studies of deep-water hazard-related features on the northern slope of South China Sea.
446 *Marine and Petroleum Geology 77, 1125-1139.*

447 Chen, H., Xie, X., Rooij, D.V., Vandorpe, T., Su, M., Wang, D., 2014. Depositional characteristics and processes
448 of along slope currents related to a seamount on the northwestern margin of the Northwest Sub-Basin, South
449 China Sea. *Mar. Geol. 355, 36–53.*

450 Gong, C.L., Wang, Y.M., Zhu, W.L., Li, W.G., Xu, Q., 2013. Upper Miocene to Quaternary unidirectionally
451 migrating deep-water channels in the Pearl River Mouth Basin, northern South China Sea. *AAPG Bull. 97,*
452 *285–308.*

453 Contreras-Rosales, L.A., Jennerjahn, T., Steinke, S., Mohtadi, M., Schefuß, E., 2019. Holocene changes in biome
454 size and tropical cyclone activity around the Northern South China Sea. *Quaternary Science Reviews 215,*
455 *45-63.*

456 Covault, J.A., Kostic, S., Paull, C.K., Ryan, H.F., Fildani, A., 2014. Submarine channel initiation, filling and
457 maintenance from sea-floor geomorphology and morphodynamic modelling of cyclic steps. *Sedimentology*
458 *61, 1031-1054.*

459 Ercilla, G., Wynn, R.B., Alonso, B., Baraza, J., 2002. Initiation and evolution of turbidity current sediment waves

460 in the Magdalena turbidite system. *Marine Geology* 192, 153-169.

461 García, M., Hernández-Molina, F.J., Llave, E., Stow, D.A.V., León, R., Fernández-Puga, M.C., Diaz del Río, V.,
462 Somoza, L., 2009. Contourite erosive features caused by the Mediterranean Outflow Water in the Gulf of
463 Cadiz: Quaternary tectonic and oceanographic implications. *Marine Geology* 257, 24-40.

464 Gee, M.J.R., Gawthorpe, R.L., Bakke, K., Friedmann, S.J., 2007. Seismic Geomorphology and Evolution of
465 Submarine Channels from the Angolan Continental Margin. *Journal of Sedimentary Research* 77, 433-446.

466 Georgiopoulou, A., Masson, D.G., Wynn, R.B., Krastel, S., 2010. Sahara Slide: Age, initiation, and processes of a
467 giant submarine slide. *Geochemistry, Geophysics, Geosystems* 11 (7): Q07014.

468 Gong, C., Wang, Y., Peng, X., Li, W., Qiu, Y., Xu, S., 2012. Sediment waves on the South China Sea Slope off
469 southwestern Taiwan: Implications for the intrusion of the Northern Pacific Deep Water into the
470 South China Sea. *Marine and Petroleum Geology* 32, 95-109.

471 Gong, C., Wang, Y., Rebesco, M., Salon, S. & Steel, R.J. 2018. How do turbidity flows interact with contour
472 currents in unidirectionally migrating deep-water channels? *Geology*, 46, 551–554.

473 Gong, C., Wang, Y., Xu, S., Pickering, K.T., Peng, X., Li, W., Yan, Q., 2015. The northeastern South China Sea
474 margin created by the combined action of downslope and along-slope processes: Processes, products and
475 implications for exploration and paleoceanography. *Marine and Petroleum Geology* 64, 233-249.

476 Gong, C., Wang, Y., Zhu, W., Li, W., Xu, Q., 2013. Upper Miocene to Quaternary unidirectionally migrating
477 deep-water channels in the Pearl River Mouth Basin, northern South China Sea. *AAPG Bull.* 97, 285–308.

478 Gong, Z.S., Jin, Q., Qiu, Z., Wang, S., Meng, J., 1989. Geology tectonics and evolution of the Pearl River Mouth
479 Basin. In: Zhu, X. (Ed.), *Chinese sedimentary basins*: Amsterdam. Elsevier, Netherlands, pp. 181–196.

480 Haflidason, H., Sejrup, H.P., Nygård, A., Mienert, J., Bryn, P., Lien, R., Forsberg, C.F., Berg, K., Masson, D.,
481 2004. The Storegga Slide: architecture, geometry and slide development. *Marine Geology* 213, 201-234.

482 He, Y., Xie, X., Kneller, B.C., Wang, Z., Li, X., 2013. Architecture and controlling factors of canyon fills on the

483 shelf margin in the Qiongdongnan Basin, northern South China Sea. *Marine and Petroleum Geology* 41,
484 264-276.

485 He, Y., Zhong, G., Wang, L., Kuang, Z., 2014. Characteristics and occurrence of submarine canyon-associated
486 landslides in the middle of the northern continental slope, South China Sea. *Marine and Petroleum Geology*
487 57, 546-560.

488 Hernández-Molina, F.J., Llave, E., Stow, D.A.V., García, M., Somoza, L., Vázquez, J.T., Lobo, F.J., Maestro, A.,
489 Díaz del Río, V., León, R., Medialdea, T., Gardner, J., 2006. The contourite depositional system of the Gulf
490 of Cádiz: A sedimentary model related to the bottom current activity of the Mediterranean outflow water and
491 its interaction with the continental margin. *Deep Sea Research Part II: Topical Studies in Oceanography* 53,
492 1420-1463.

493 Jobe, Z.R., Lowe, D.R., Uchytel, S.J., 2011. Two fundamentally different types of submarine canyons along the
494 continental margin of Equatorial Guinea. *Marine and Petroleum Geology* 28, 843-860.

495 Laberg, J.S., Guidard, S., Mienert, J., Vorren, T.O., Haflidason, H., Nygård, A., 2007. Morphology and
496 morphogenesis of a high-latitude canyon; the Andøya Canyon, Norwegian Sea. *Marine Geology* 246, 68–85.

497 Li, C.-F., Li, J., Ding, W., Franke, D., Yao, Y., Shi, H., Pang, X., Cao, Y., Lin, J., Kulhanek, D.K., Williams, T.,
498 Bao, R., Briais, A., Brown, E.A., Chen, Y., Clift, P.D., Colwell, F.S., Dadd, K.A., Hernández-Almeida, I.,
499 Huang, X.-L., Hyun, S., Jiang, T., Koppers, A.A.P., Li, Q., Liu, C., Liu, Q., Liu, Z., Nagai, R.H.,
500 Peleo-Alampay, A., Su, X., Sun, Z., Tejada, M.L.G., Trinh, H.S., Yeh, Y.-C., Zhang, C., Zhang, F., Zhang,
501 G.-L., Zhao, X., 2015a. Seismic stratigraphy of the central South China Sea basin and implications for
502 neotectonics. *Journal of Geophysical Research: Solid Earth* 120, 1377-1399.

503 Li, W., Alves, T.M., Wu, S., Völker, D., Zhao, F., Mi, L., Kopf, A., 2015b. Recurrent slope failure and submarine
504 channel incision as key factors controlling reservoir potential in the South China Sea (Qiongdongnan Basin,
505 South Hainan Island). *Marine and Petroleum Geology* 64, 17-30.

506 Li, W., Krastel, S., Alves, T.M., Urlaub, M., Mehringer, L., Schürer, A., Feldens, P., Gross, F., Stevenson, C.J.,
507 Wynn, R.B., 2018. The Agadir Slide offshore NW Africa: Morphology, emplacement dynamics, and potential
508 contribution to the Moroccan Turbidite System. *Earth and Planetary Science Letters* 498, 436-449.

509 Li, W., Wu, S.G., Völker, D., Zhao, F., Mi, L.J., Kopf, A., 2014. Morphology, seismic characterization and
510 sediment dynamics of the Baiyun slide complex on the northern South China Sea margin. *J. Geol. Soc. Lond.*
511 171, 865–877.

512 Lonergan, L., Jamin, N.H., Jackson, C.A.L., Johnson, H.D., 2013. U-shaped slope gully systems and sediment
513 waves on the passive margin of Gabon (West Africa). *Marine Geology* 337, 80-97.

514 Lüdmann, T., Wong, H.K., Berglar, K., 2005. Upward flow of North Pacific Deep Water in the northern South
515 China Sea as deduced from the occurrence of drift sediments. *Geophysical Research Letters* 32.

516 Ma, B., Wu, S., Sun, Q., Mi, L., Wang, Z., Tian, J., 2015. The late Cenozoic deep-water channel system in the
517 Baiyun Sag, Pearl River Mouth Basin: Development and tectonic effects. *Deep Sea Research Part II: Topical*
518 *Studies in Oceanography* 122, 226-239.

519 Martorelli E., Bosman A., Casalbore D., Chiocci F.L., Falcini F. (2016) Interaction of down-slope and along-slope
520 processes off Capo Vaticano (southern Tyrrhenian Sea, Italy), with particular reference on contourite-related
521 landslides. *Marine Geology*, 378: 43-55.

522 Micallef, A., Mountjoy, J.J., 2011. A topographic signature of a hydrodynamic origin for submarine gullies.
523 *Geology* 39, 115-118.

524 Moscardelli, L., Wood, L., Mann, P., 2006. Mass-transport complexes and associated processes in the offshore
525 area of Trinidad and Venezuela. *AAPG Bulletin* 90, 1059-1088.

526 Mosher, D.C., Campbell, D.C., Gardner, J.V., Piper, D.J.W., Chaytor, J.D., Rebesco, M., 2017. The role of
527 deep-water sedimentary processes in shaping a continental margin: The Northwest Atlantic. *Marine Geology*
528 393, 245-259.

529 Normark, W.R., Piper, D.J.W., Posamentier, H., Pirmez, C., Migeon, S., 2002. Variability in form and growth of
530 sediment waves on turbidite channel levees. *Marine Geology* 192, 23-58.

531 Pubellier, M., Ego, F., Chamot-Rooke, N., Rangin, C., 2003. The building of pericratonic mountain ranges:
532 structural and kinematic constraints applied to GIS-based reconstructions of SE Asia. *Bull. de la Société*
533 *géologique de France* 174 (6), 561-584.

534 Qin, Y., Alves, T., Constantine, J.A., Gamboa, D., 2017. The role of mass wasting in the progressive
535 development of submarine channels (Espírito Santo Basin, SE Brazil). *J. Sediment. Res.*, 87, 500-516.

536 Rebesco, M., Özmaral, A., Urgeles, R., Accettella, D., Lucchi, R.G., Rütther, D., Winsborrow, M., Llopart, J.,
537 Caburlotto, A., Lantzsch, H., Hanebuth, T.J.J., 2016. Evolution of a high-latitude sediment drift inside a
538 glacially-carved trough based on high-resolution seismic stratigraphy (Kveithola, NW Barents Sea).
539 *Quaternary Science Reviews* 147, 178-193.

540 Rebesco, M., Camerlenghi, A., Volpi, V., Neagu, C., Accettella, D., Lindberg, B., Cova, A., Zgur, F., 2007.
541 Interaction of processes and importance of contourites: insights from the detailed morphology of sediment
542 Drift 7, Antarctica. *Geological Society, London, Special Publications* 276, 95.

543 Rebesco, M., Hernández-Molina, F.J., Van Rooij, D., Wåhlin, A., 2014. Contourites and associated sediments
544 controlled by deep-water circulation processes: State-of-the-art and future considerations. *Marine Geology*
545 352, 111-154.

546 Rebesco, M., Pudsey, C.J., Canals, M., Camerlenghi, A., Barker, P.F., Estrada, F., Giorgetti, A., 2002. Sediment
547 drifts and deep-sea channel systems, Antarctic Peninsula Pacific Margin. *Geological Society, London,*
548 *Memoirs* 22, 353.

549 Rebesco, M., Wåhlin, A., Laberg, J.S., Schauer, U., Beszczynska-Möller, A., Lucchi, R.G., Noormets, R.,
550 Accettella, D., Zarayskaya, Y., Diviacco, P., 2013. Quaternary contourite drifts of the Western Spitsbergen
551 margin. *Deep Sea Research Part I: Oceanographic Research Papers* 79, 156-168.

552 Shepard, F. P., 1936. The Underlying Causes of Submarine Canyons: Proceedings of the National Academy of
553 Sciences of the United States of America, 22 (8), 496-502.

554 Shepard, F.P., 1981. Submarine canyons; multiple causes and long-time persistence. Am. Assoc. Petrol. Geol. Bull.
555 65: 1062–1077.

556 Steinke, S., Chiu, H.-Y., Yu, P.-S., Shen, C.-C., Erlenkeuser, H., Löwemark, L., Chen, M.-T., 2006. On the
557 influence of sea level and monsoon climate on the southern South China Sea freshwater budget over the last
558 22,000 years. Quaternary Science Reviews 25, 1475-1488.

559 Steinke, S., Groeneveld, J., Johnstone, H., Rendle-Bühning, R., 2010. East Asian summer monsoon weakening
560 after 7.5Ma: Evidence from combined planktonic foraminifera Mg/Ca and $\delta^{18}O$ (ODP Site 1146; northern
561 South China Sea). Palaeogeography, Palaeoclimatology, Palaeoecology 289, 33-43.

562 Steinke, S., Kienast, M., Hanebuth, T., 2003. On the significance of sea-level variations and shelf
563 paleo-morphology in governing sedimentation in the southern South China Sea during the last deglaciation.
564 Marine Geology 201, 179-206.

565 Sun, Q., Alves, T. M., Lu, X., Chen, C., and Xie, X., 2018a. True Volumes of Slope Failure Estimated From a
566 Quaternary Mass-Transport Deposit in the Northern South China Sea: Geophysical Research Letters, 45 (6),
567 2642-2651.

568 Sun, Q., Cartwright, J., Xie, X., Lu, X., Yuan, S., Chen, C., 2018b. Reconstruction of repeated Quaternary slope
569 failures in the northern South China Sea. Marine Geology 401, 17-35.

570 Sun, Q., Xie, X., Piper, D.J.W., Wu, J., Wu, S., 2017. Three dimensional seismic anatomy of multi-stage mass
571 transport deposits in the Pearl River Mouth Basin, northern South China Sea: Their ages and kinematics.
572 Marine Geology 393, 93-108.

573 Surlyk, F., Lykke-Andersen, H., 2007. Contourite drifts, moats and channels in the Upper Cretaceous chalk of the
574 Danish Basin. Sedimentology 54, 405-422

575 Tian, J., Yang, Q., Liang, X., Xie, L., Hu, D., Wang, F., Qu, T., 2006. Observation of Luzon Strait transport.
576 *Geophys. Res. Lett.* 33, L19607.

577 Vandorpe, T., Martins, I., Vitorino, J., Hebbeln, D., García, M., Van Rooij, D., 2016. Bottom currents and their
578 influence on the sedimentation pattern in the El Arraiche mud volcano province, southern Gulf of Cadiz.
579 *Marine Geology* 378, 114-126.

580 Vorren, T.O., Laberg, J.S., Blaume, F., Dowdeswell, J.A., Kenyon, N.H., Mienert, J., Rumohr, J.A.N., Werner, F.,
581 1998. The Norwegian–Greenland Sea continental margins: Morphology and Late Quaternary sedimentary
582 processes and environment. *Quaternary Science Reviews* 17, 273-302.

583 Wang, X., Wang, Y., He, M., Chen, W., Zhuo, H., Gao, S., Wang, M., and Zhou, J., 2017, Genesis and evolution of
584 the mass transport deposits in the middle segment of the Pearl River canyon, South China Sea: Insights from
585 3D seismic data: *Marine and Petroleum Geology*, v. 88, p. 555-574.

586 Wang, X., Zhuo, H., Wang, Y., Mao, P., He, M., Chen, W., Zhou, J., Gao, S., Wang, M., 2018. Controls of contour
587 currents on intra-canyon mixed sedimentary processes: Insights from the Pearl River Canyon, northern South
588 China Sea. *Marine Geology* 406, 193-213.

589 Wu, S., Gao, J., Zhao, S., Lüdmann, T., Chen, D., Spence, G., 2014. Post-rift uplift and focused fluid flow in the
590 passive margin of northern South China Sea. *Tectonophysics* 615-616, 27-39.

591 Wynn, R.B., Stow, D.A.V., 2002. Classification and characterisation of deep-water sediment waves. *Marine*
592 *Geology* 192, 7-22.

593 Xie, X., Müller, R.D., Li, S., Gong, Z., Steinberger, B., 2006. Origin of anomalous subsidence along the Northern
594 South China Sea margin and its relationship to dynamic topography. *Marine and Petroleum Geology* 23,
595 745-765.

596 Zhao, F., Alves, T.M., Li, W., Wu, S., 2015. Recurrent slope failure enhancing source rock burial depth and seal
597 unit competence in the Pearl River Mouth Basin, offshore South China Sea. *Tectonophysics* 643, 1-7.

598 Zhao, F., Alves, T.M., Wu, S., Li, W., Huuse, M., Mi, L., Sun, Q., Ma, B., 2016. Prolonged post-rift magmatism on
599 highly extended crust of divergent continental margins (Baiyun Sag, South China Sea). *Earth and Planetary
600 Science Letters* 445, 79-91.

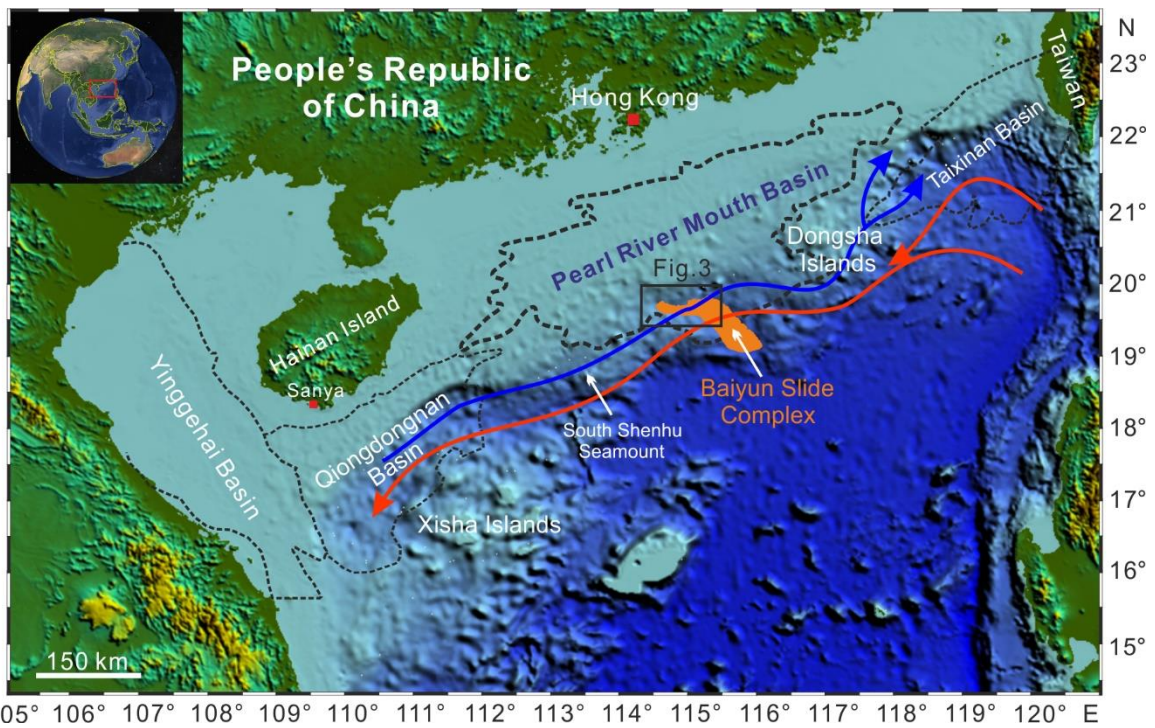
601 Zhao, W., Zhou, C., Tian, J.W., Yang, Q.X., Wang, B., Xie, L.L., Qu, T.D., 2014. Deep water circulation in the
602 Luzon Strait. *J. Geophys. Res. Oceans* 119, 790-804.

603 Zhu, M., Graham, S., Pang, X., McHargue, T., 2010. Characteristics of migrating submarine canyons from the
604 middle Miocene to present: Implications for paleoceanographic circulation, northern South China Sea.
605 *Marine and Petroleum Geology* 27, 307-319.

606

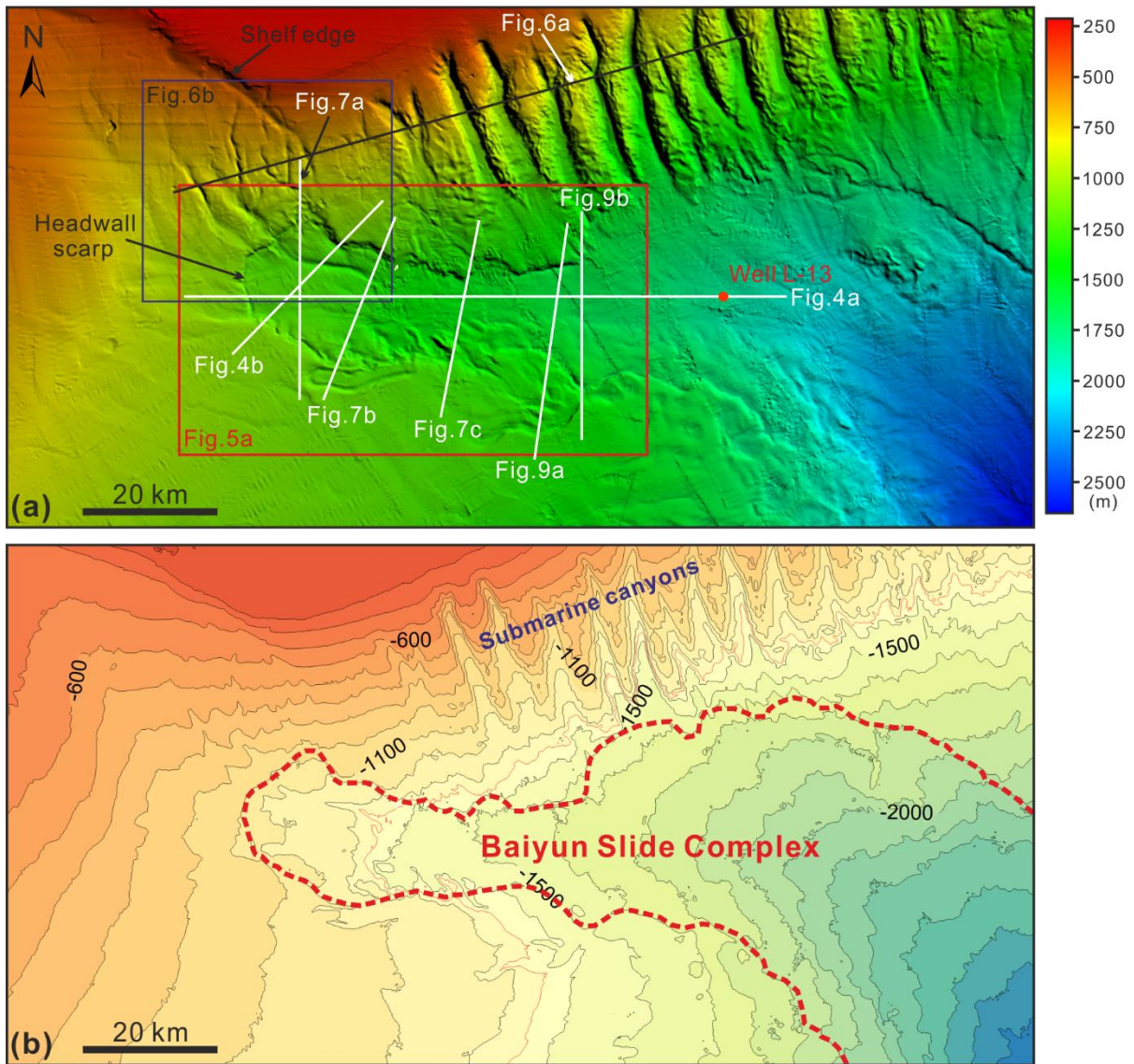
607

608 **Figure Captions**



609

610 Fig.1 Seafloor physiography of the northern South China Sea margin showing the distribution of the
611 major sedimentary basins and geomorphological features (e.g. Dongsha Islands, Xisha Islands and
612 South Shenhu Seamount). The blue and red curves indicate the paths of intermediate and deep water
613 offshore the northern South China Sea (Tian et al., 2006; Chen et al., 2014). The location of the
614 Baiyun Slide Complex is marked in orange (Li et al., 2014). The black box indicates the location of
615 the study area (see Fig. 2).



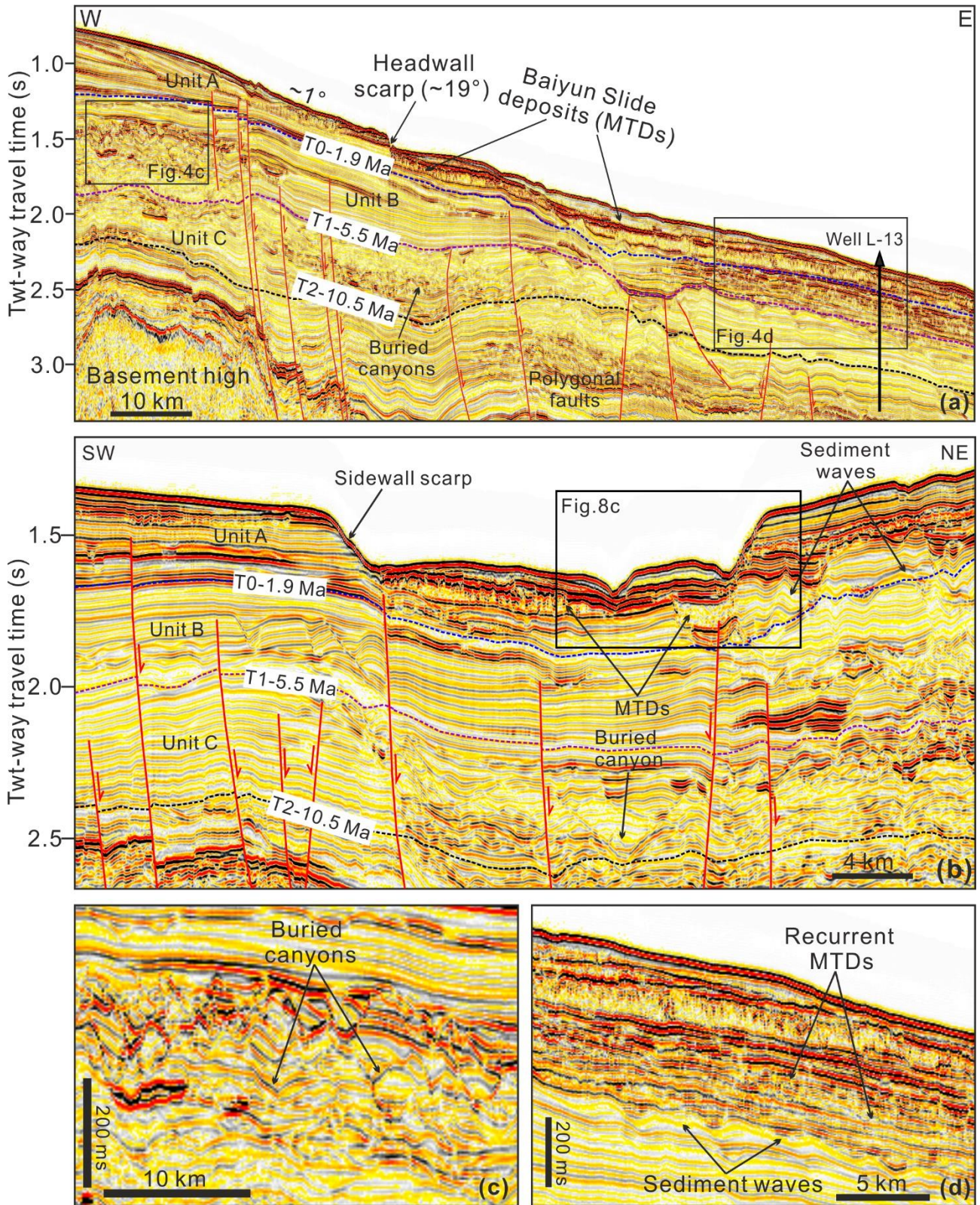
616
 617 Fig. 2 (a) Multibeam bathymetry map of the study area illustrating the seafloor morphology of the
 618 headwall region of Baiyun Slide Complex, and multiple submarine canyons. The white lines reveal
 619 the location of seismic lines interpreted in this paper. The red box indicates the location of the
 620 headwall region of the Baiyun Slide Complex, which is highlighted in Fig. 5a. The location of Fig.
 621 6b is marked by the purple box. (b) Contour map of the study area. The contour interval is 100 m.
 622 The red dashed line indicates the boundary of the Baiyun Slide Complex. Please see the location of
 623 Fig. 2 in Fig. 1.

Epoch	Formation	Seismic Reflector	Age (Ma)	Regional Tectonic Events	Sedimentary Environment	
Quaternary						
Pliocene	Wanshan	T0	1.9			
Miocene	Upper	Yuehai	T1	5.5	Dongsha Event	Deep-water continental slope sedimentary environment
	Middle	Hanjiang	T2	10.5		
			T3	13.8		
	Lower	Zhujiang	T4	16.5		
		T5	18.5			
Oligocene	Upper	Zhuhai	T6	23.5	Baiyun Event	Shallow-water shelf
	Lower	Enping	T7	30	Nanhai Event	
Paleocene ~ Eocene	Upper			T8	39	
	Middle	Wenchang				
		Shenhu	Tg			

624

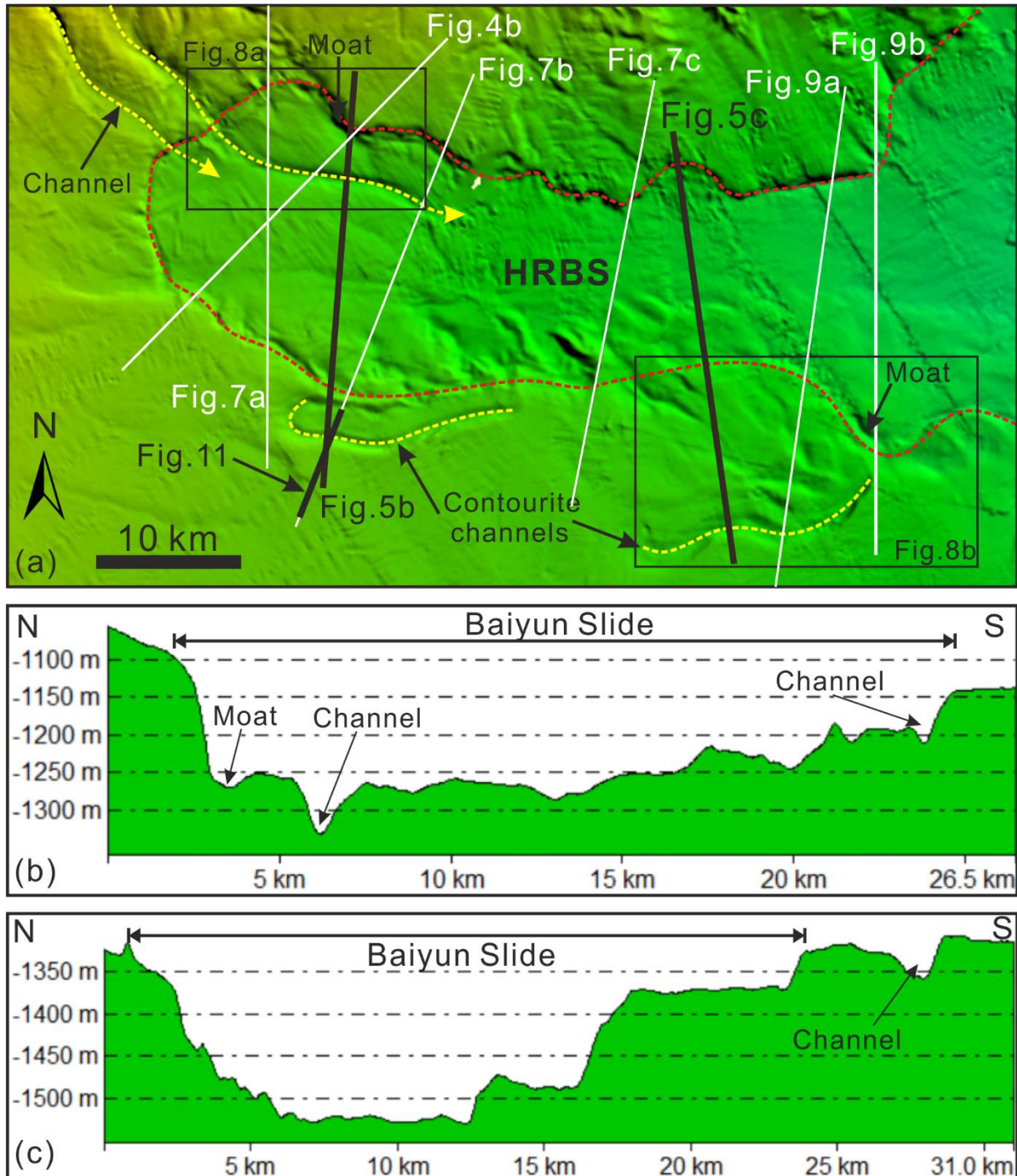
625 Fig. 3 Schematic stratigraphic columns of the Pearl River Mouth Basin showing the main regional
626 tectonic events and sedimentary environments (modified after Zhao et al., 2015).

627



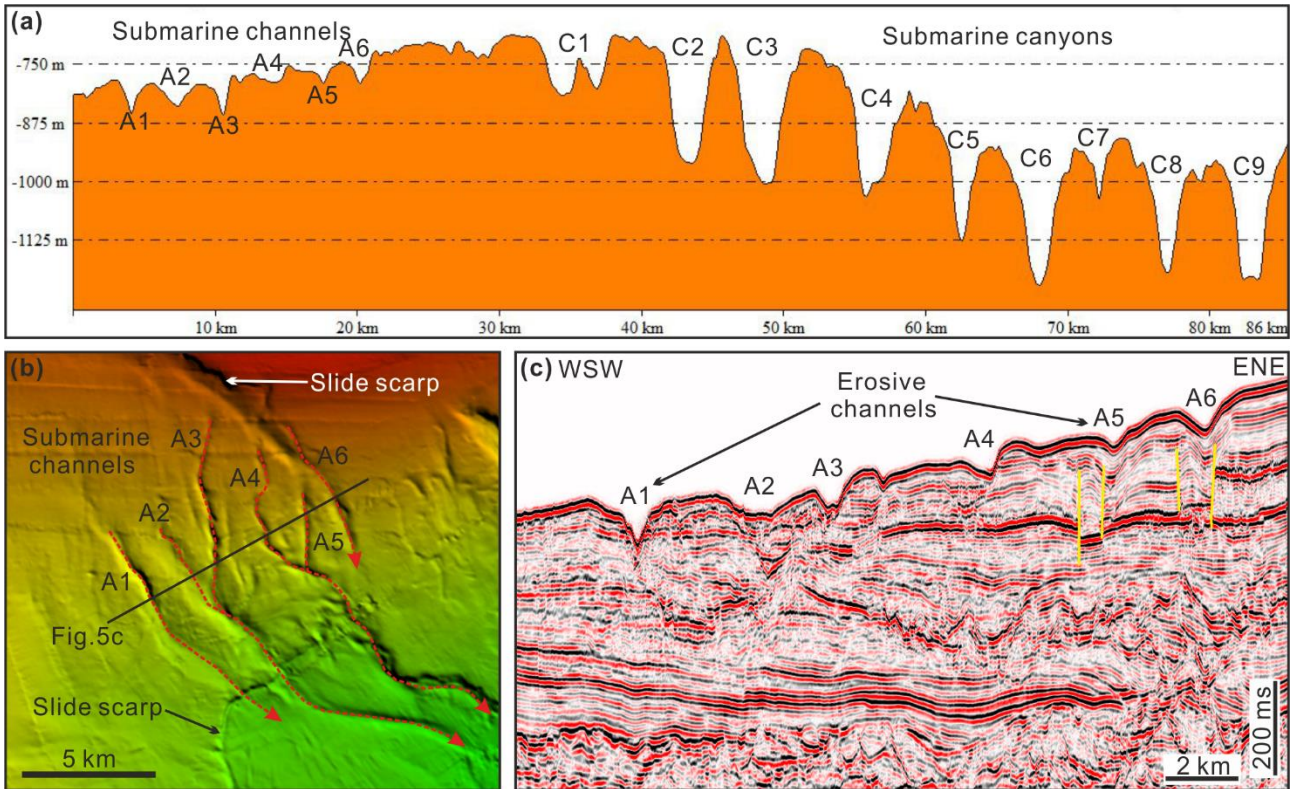
628
 629 Fig. 4 (a) Three-dimensional seismic profile crossing the headwall region of Baiyun Slide Complex
 630 and showing details of the headwall scarp and corresponding mass-transport deposits (MTDs) on
 631 the lower continental slope. (b) Zoomed in seismic profile (see location in Fig. 6a) revealing the

632 presence of sediment waves beneath MTDs. (c) Zoomed in seismic profile in the lower continental
 633 slope below the headwall region. The profile illustrates the presence of recurrent MTDs. Please see
 634 the location of Fig. 4 in Fig. 2.

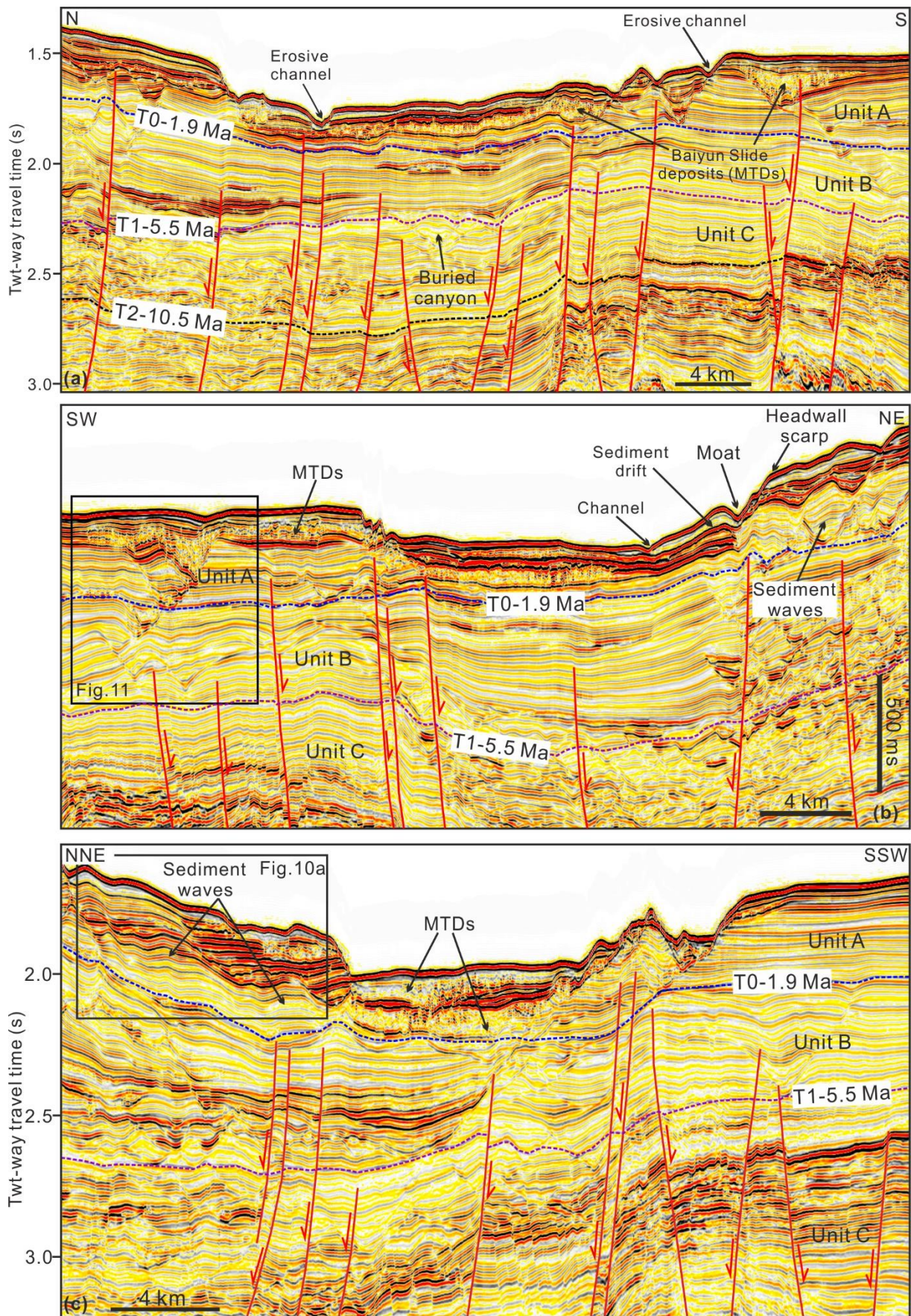


635
 636 Fig.5 (a) Multibeam bathymetric map showing the detailed seafloor morphology of the headwall
 637 region of the Baiyun Slide Complex. The escarpment in the headwall region of the Baiyun Slide is
 638 marked by a red dashed line. The yellow dashed lines indicate the locations of submarine channels

639 on the modern sea floor. The black solid lines represent the bathymetric profiles in Figs. 5b and 5c.
 640 Please see the location of Fig. 5a in Fig. 2a. (b) Bathymetric profile crossing the headwall region of
 641 the Baiyun Slide and revealing the presence of submarine channels. (c) Bathymetric profile
 642 revealing the presence of submarine channels in the headwall region. HRBS: headwall region of the
 643 Baiyun Slide.



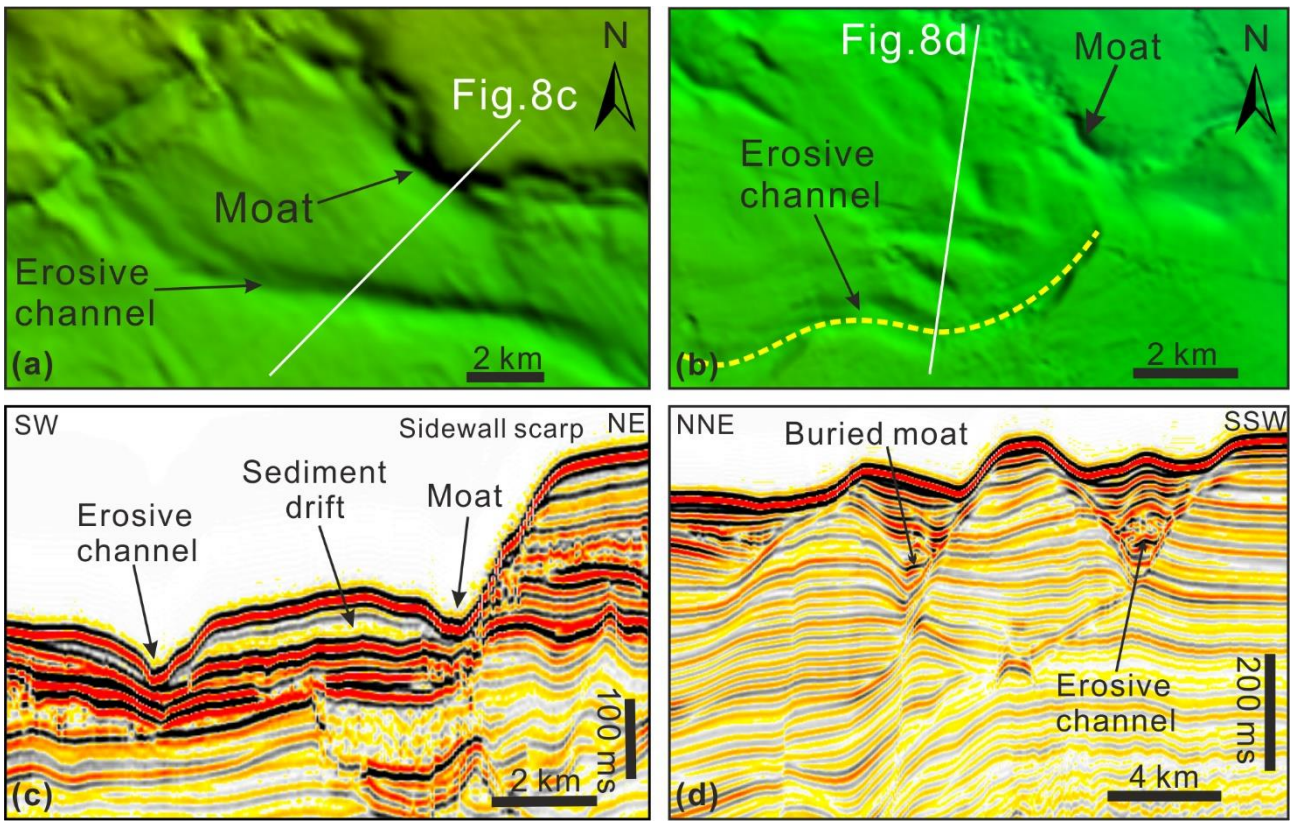
644
 645 Fig. 6 (a) Bathymetric profile crossing submarine canyons C1 to C9 and submarine channels A1 to
 646 A6 in the upper continental slope region of the Baiyun Slide Complex (see location in Fig. 3). Note
 647 that submarine canyons (C1 to C9) show much larger incision depths than submarine channels A1
 648 to A6. Please see the location of Fig. 6a in Fig. 3a. (b) Multibeam bathymetric map showing the
 649 detailed seafloor morphology of submarine channels A1 to A6. (c) Two-dimensional seismic profile
 650 revealing the internal architecture of submarine channels above the headwall region of the Baiyun
 651 Slide Complex. See location of the seismic profile in Fig. 6b.



652

653 Fig. 7 Three high-resolution seismic profiles crossing different locations of the headwall region to

654 reveal its detailed internal architecture. (a) 3D seismic line showing the presence of buried
655 submarine canyons, MTDs, large-scale faults and erosive channels on the modern sea floor. (b) A
656 moat and buried sediment waves can be identified in the northern part of the headwall region. A
657 migrating channel is located in the southern part of the headwall region, as shown in detail in Fig.
658 11a. (c) 3D seismic profile reveals the presence of sediment waves in the northern part of the
659 headwall region, as shown in detail in Fig. 10a. Please see the location of Fig. 7 in Figs. 2a and 5a.
660



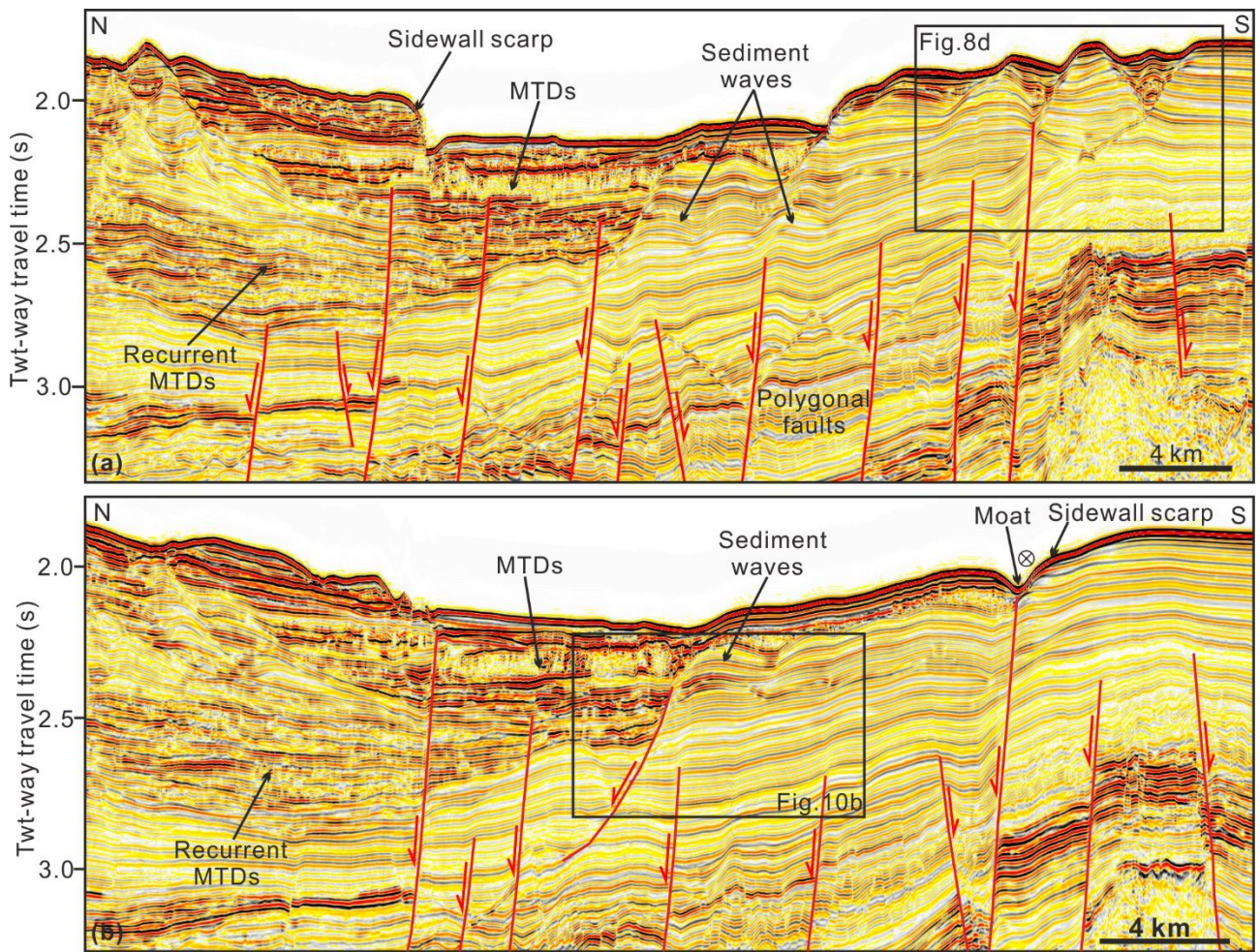
661

662

663

664

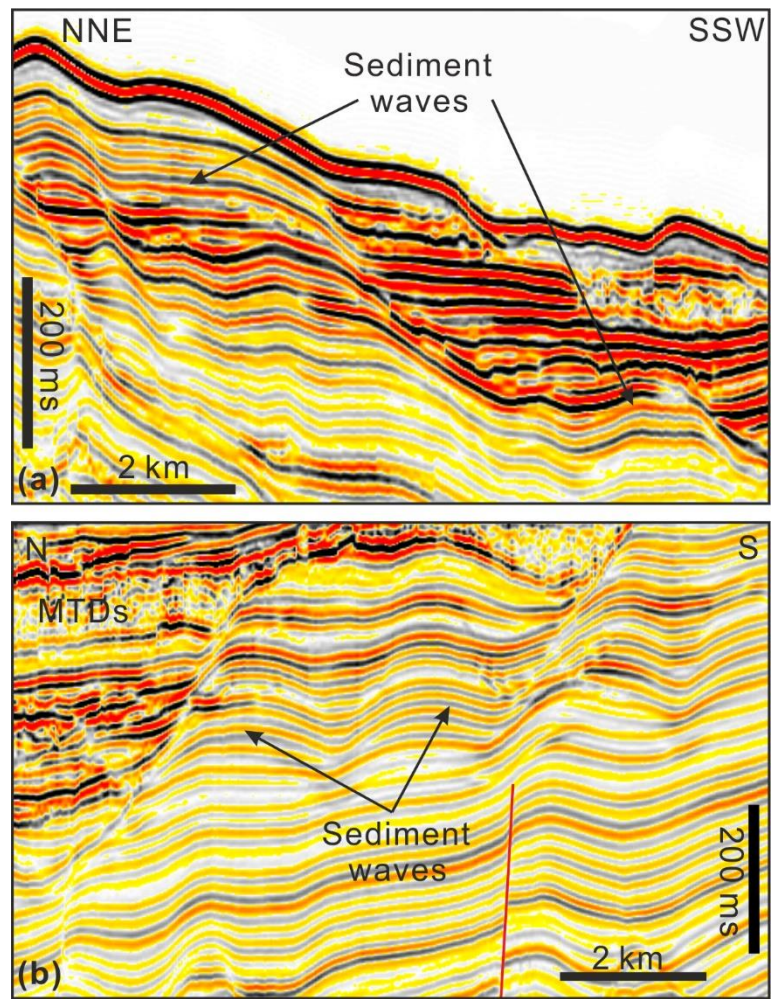
Fig. 8 Enlarged seismic sections (a-d) illustrating the moat and sediment drift developed close to the southern sidewall scarp of the Baiyun Slide Complex. Erosive channels and related truncations can be observed on the modern sea floor.



665

666 Fig. 9 (a) 3D seismic line crossing the eastern part of the headwall region showing sediment waves
 667 buried by recurrent MTDs. A buried moat and a submarine channel can be observed in the southern
 668 part of the headwall region. (b) 3D seismic line illustrating a moat close to the sidewall scarp of the
 669 Baiyun Slide. A large-scale fault nearly propagates to the sea floor. Please see the location of Fig. 9
 670 in Figs. 2a and 5a.

671

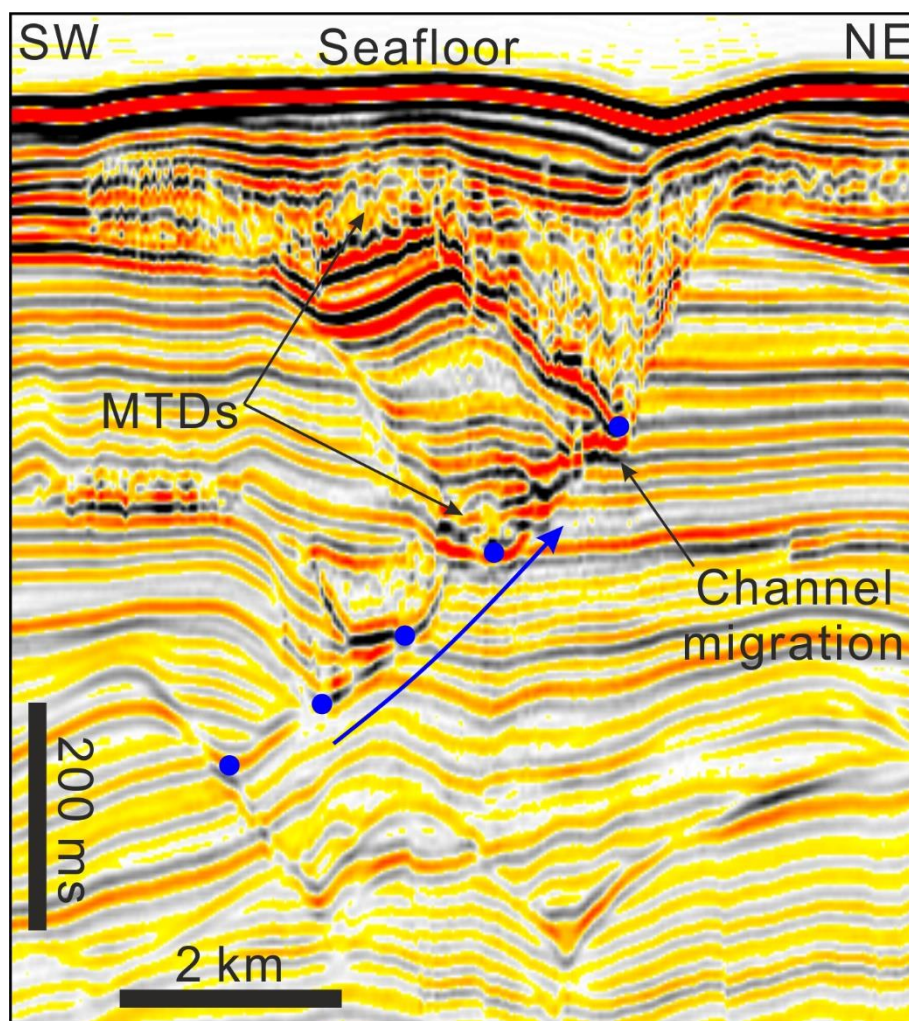


672

673 Fig. 10 (a) Zoomed-in seismic profile showing the internal architecture of sediment waves in the
 674 northern part of the headwall region, close to the submarine canyons on the upper continental slope.

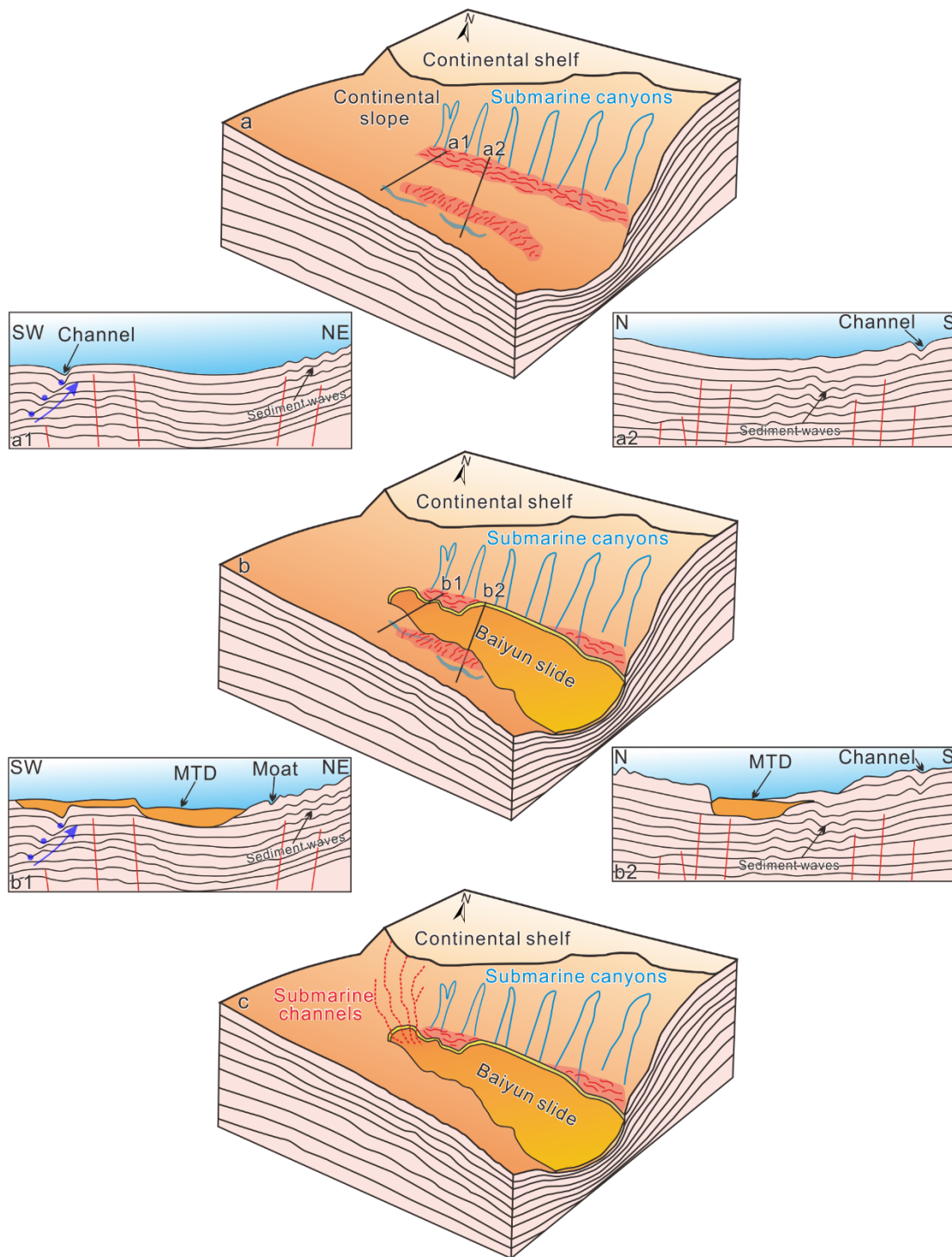
675 See location of the profile in Fig. 7. (b) Zoomed in seismic profile revealing the presence of
 676 sediment waves in the southern part of the headwall region. See location of the seismic profile in

677 Fig. 9b.



678

679 Fig. 11 Interpreted seismic profile from the southern part of the headwall region revealing a buried
 680 submarine channel. The blue dots represent the base of the buried channel, which reveal a N-S
 681 migration trend at start to then migrate towards the north. Please see the location of Fig. 11 in Fig.
 682 5a.



683

684 Fig. 12 Conceptual model showing the morphological evolution inside and around the Baiyun Slide
 685 scar. (a) The continental slope was incised by several submarine canyons. The sediment waves in
 686 the north were formed by turbidity currents flowing through the submarine canyons (a1), while
 687 those in the south resulted from the interaction of bottom currents with the seafloor (a2). A
 688 submarine channel shows an obvious migration pattern towards northeast (b) The Baiyun Slide

689 occurred downslope from the submarine canyons and it evacuated large volumes of sediment
 690 (~1035 km³) on the sea floor. The Baiyun Slide eroded the sediment wave fields and the resulted
 691 MTDs filled the migrating channel in the south (b1 and b2). (c) Several submarine channels were
 692 formed after the Baiyun Slide Complex to erode the headwall scarps of the Baiyun Slide Complex.

693

Channels	A1	A2	A3	A4	A5	A6
Width (m)	~900	~1500	~800	~1000	~900	~1400
Length (km)	~24	~33	~37	~32	~26	~16
Incised Depth (m)	~73	~22	~52	~34	~42	41
SW Flank (°)	~10	~3	~7	~4	~7	~3
NE Flank (°)	~11	~5	~16	~7	~8	~4

694 Table 1 Morphological parameters, including widths, lengths, incised depths, dipping angles of the
 695 southwestern (SW) and northeastern (NE) flanks, of the submarine channels identified in the
 696 upslope region of Baiyun Slide scar.